Recent Development in the Operational Regime of Large Helical Device Toward a Steady-State Helical Fusion Reactor

Y. Takeiri, A. Komori, H. Yamada, K. Kawahata, T. Mutoh, N. Ohyabu, O. Kaneko, S. Imagawa, Y. Nagayama, K.Y. Watanabe, T. Shimozuma, K. Ida, R. Sakamoto, M. Kobayashi, A. Sagara, K. Nagaoka, M. Yoshinuma, S. Sakakibara, Y. Suzuki, M. Yokoyama, S. Sudo, O. Motojima, and LHD experimental Group

National Institute for Fusion Science, 322-6 Oroshi-cho, Toki 509-5292, Japan

(Received 29 October 2007 / Accepted 29 October 2007)

Recent progress of the plasma performance and the related physics understanding is overviewed in Large Helical Device. The volume-averaged beta value is increased with an increase in the NBI heating power, and reached 5.0% of the reactor-relevant value. In the high-β plasmas, the plasma aspect ratio should be controlled so that the Shafranov shift would be reduced mainly to suppress the transport degradation and the deterioration of NBI heating efficiency. The operational regime of the high-density plasma with internal diffusion barrier (IDB) has been extended, and the IDB, which was originally found by use of the local island divertor, has been realized in the helical divertor configuration. The central density was recorded as high as $1x10^{21}m^{-3}$, and the central pressure reached 130kPa. Based on these high-density plasmas with the IDB, a new ignition scenario has been proposed. This should be a specific scenario to the helical fusion reactor, in which the helical ripple transport would be mitigated. A low-energy positive-NBI system was newly installed for an increase in the direct ion heating power. As a result, the T_i exceeded 5.2keV at a density of $1.2x10^{19}m^{-3}$ in the hydrogen plasma. The T_i-increase tends to be accompanied by a large toroidal rotation velocity of the order of 50km/s in the core region. The plasma properties in the extended operational regime are discussed with regard to a perspective to the steady-state helical fusion reactor.

Keywords: Large Helical Device, MHD stability, Shafranov shift, internal diffusion barrier, ion transport, toroidal rotation, impurity hall, helical fusion reactor, neoclassical transport, anomalous transport, core electron-root confinement

1. Introduction

The Large Helical Device (LHD) is the world's largest superconducting helical device, which started its operation in 1998 [1-3]. The objective of LHD is to demonstrate high performance of net-current free heliotron plasmas relevant to the steady-state helical fusion reactor. During the nine years' operation, LHD has exploited novel operational regimes related to plasma confinement, MHD stability and steady-state operation, including plasma-wall interaction [4,5].

Recently, much progress of the plasma performance has been achieved together with the physics understanding, which was mainly brought by the upgrade of the heating systems. The volume-averaged β value is increased with an increase in the NB injection power, and reached 5% as a consequence of the enhancement of the negative-NBI power to 14MW. A low-energy positive-NBI system has been installed recently for an increase in the direct ion heating power, and, as a result, the T_i exceeded 5.2keV at a density of $1.2x10^{19}m^{-3}$ in a hydrogen plasma. The distinguished feature found in LHD is the formation of the internal diffusion barrier (IDB) [6], which is realized by combination of efficient pumping with the local island divertor (LID) [7] and core fuelling with repetitive pellet injection [8], and it is sustained by the high-power NBI heating. In a super-dense core (SDC) plasma with the IDB, the central density was recorded as high as $5x10^{20}m^{-3}$ [6]. The IDB has also been observed recently in the helical divertor (HD) configuration with a well-conditioned wall. Based on the SDC/IDB plasmas, a new ignition scenario has been proposed, and this should be a specific scenario to the helical fusion reactor, in which the helical ripple transport would be mitigated [9]. Inherent advantage to steady-state operation has been demonstrated with the improvement of the ICRF and ECH heating systems. A long-pulse plasma was sustained for 54min with ICRF and

author's e-mail: takeiri@nifs.ac.jp

ECH, and the input heating energy reached 1.6GJ [10].

One of the specific characteristics in LHD is the dependence of the plasma properties, such as confinement, transport, MHD stability, and divertor structure, on the magnetic axis position. In the inward-shifted configuration, the transport including the high-energy particle confinement is improved while the MHD stability is degraded due to the enhancement of the magnetic hill region, and the tendency is reversed in the outer-shifted configuration. The most significant achievement in the LHD research is the compatibility of the transport and the MHD stability, which is realized by the sophisticated optimization of the magnetic configuration including the magnetic axis position and the control of the Shafranov shift due to the plasma pressure [11].

In this overview, we present the recent development in the operational regime of the LHD experiments, highlighting mainly topics for the high-β, high-density with IDB, and the high-T_i, and the related physics understanding is discussed with a perspective of the steady-state helical fusion reactor.

2. Large Helical Device and Heating Systems

The Large Helical Device (LHD) employs a heliotron configuration, and consists of a pair of continuous helical coils, which has an l=2/m=10 poloidal/toroidal field period, and three pairs of poloidal coils [3]. These coils are all superconducting, and provide a wide variety of the magnetic configuration by controlling the current ratio of these coils. The magnetic axis position is changed with the poloidal coils, and ranges 3.5-4.1m in the major radius in the experiments. The averaged minor radius is about 0.6m at the maximum and the corresponding plasma volume is about $30m^3$, and these are dependent on the magnetic configuration. The magnetic field strength on the axis is 3T at the maximum.

The LHD has the intrinsic helical divertor (HD), which is a sort of helically twisted double-null open divertor. Additionally, the LHD is equipped with a local island divertor (LID) system, which utilizes the m/n=1/1 magnetic island induced externally with the perturbation coils [7]. The LID facilitates the edge plasma control with highly efficient pumping capability.

The main heating system is a negative-ion-based neutral beam injection (negative-NBI) system, which consists of three tangential injectors with the nominal hydrogen-injection energy of 180keV [12,13]. The total injection power achieved is 14MW. A low-energy positive-NBI system, the injection direction of which is perpendicular to the magnetic axis, was operational in 2005, and 40keV-6MW injection has been achieved [14].

The electron cyclotron resonance heating (ECRH) system is equipped with 168GHz, 84GHz, and 82.7GHz gyrotrons, and the total injection power achieved is 2.1MW [15]. Using antenna systems with quasi-optical mirrors, each microwave is injected as a highly focused Gaussian beam, and the focused location can be changed at 3.5-3.9m of the major radius on the equatorial plane.

The ion cyclotron range of frequencies (ICRF) heating system facilitates the long-pulse operation, which is capable of a steady-state injection of 1MW with four antennas, while the achieved power is 2.9MW in a short pulse injection [16].

3. Properties of Reactor-Relevant High-β Plasmas

As described above, the LHD-plasma performance is strongly dependent on the magnetic axis position. Since the heliotron configuration has a weak magnetic shear in the core region and a magnetic hill toward the peripheral region, the linear theory indicates that the interchange mode is unstable in the inward-shifted configurations, in which the particle orbit and the transport are better. On the other hand, in the outward-shifted configurations, although the MHD mode is stable due to expansion of the magnetic well region, the particle orbit and the transport are degraded. Through the optimization of the magnetic axis position, it was found that the interchange mode in the core region is stabilized and the Mercier criterion does not prohibit the access to higher β, even in the inward-shifted configuration of R_{ax}^{vac}=3.6m by the spontaneous generation of a magnetic well due to the finite β effect [11].

However, as the β increases further, the Shafranov shift becomes larger. As a result, the transport is degraded

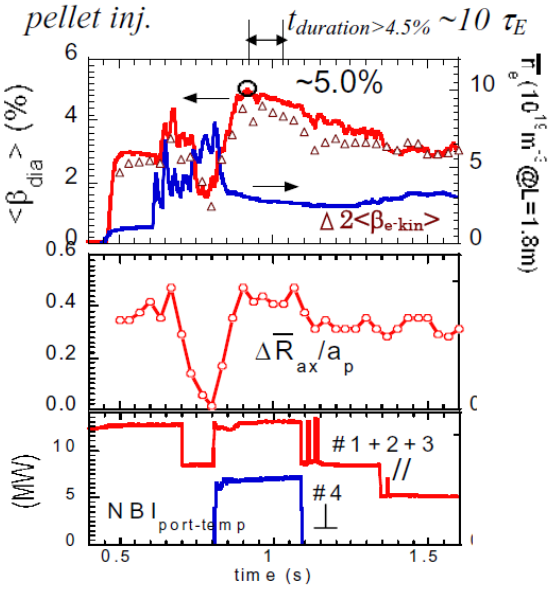

Fig.1 Waveforms in a high-β plasma of <β>=5.0% achieved with the repetitive pellet injection.

and the NBI heat deposition is deteriorated due to the enhancement of the orbit loss by the outward shift of the magnetic axis. Moreover, the large Shafranov shift lowers the MHD equilibrium beta limit. Then, the plasma aspect ratio, A_p, which can be controlled by changing the current ratio of the three layers of the helical coils, should be optimized [17]. A large A_p reduces the Shafranov shift, but an excessive increase in the A_p violates the MHD stability due to immoderate suppression of the spontaneous generation of the magnetic well. As a consequence of a series of experiments for the A_p optimization including the magnetic field strength, we have achieved 5% of the volume-averaged beta value, <β>, which is a reactor-relevant value, at A_p=6.6, B=0.425T, and preset R_{ax}^{vac}=3.6m with an increased NBI absorbed power of 11MW.

Figure 1 shows discharge waveforms in the high-β plasma of <β>=5.0% achieved with a pellet injection. The tangential NBI power is reduced in the repetitive pellet injection phase for effective penetration of the pellets. At that time, the Shafranov shift is rapidly reduced, and then the perpendicular NBI is injected together with the restoration of the tangential NBI immediately after the end of the pellet injection. Due to the reduction of the Shafranov shift, the perpendicularly injected beam effectively heats the plasma, and the <β> is rapidly increased, then reaching 5%. Although <β>=5% was transiently achieved due to the effective fueling by the pellet injection and the effective heating by the perpendicular NBI during the reduction of the Shafranov shift, no crucial MHD instability was observed in a period of 10 times the confinement time, during which the <β> was over 4.5%.

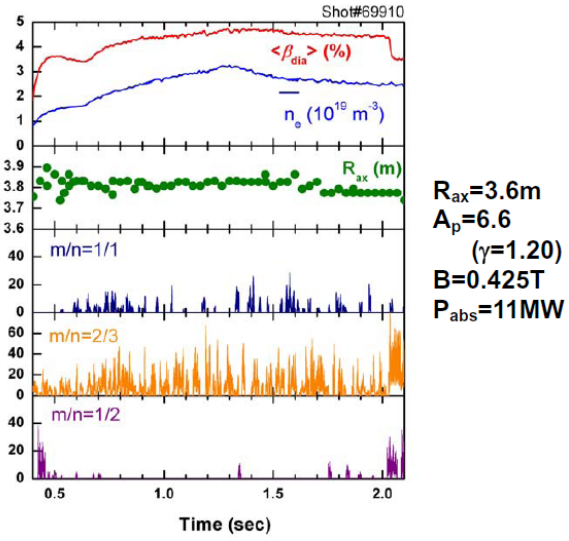

Fig.2 Waveforms in the stationary sustained high <β> plasma with only the gas puffing.

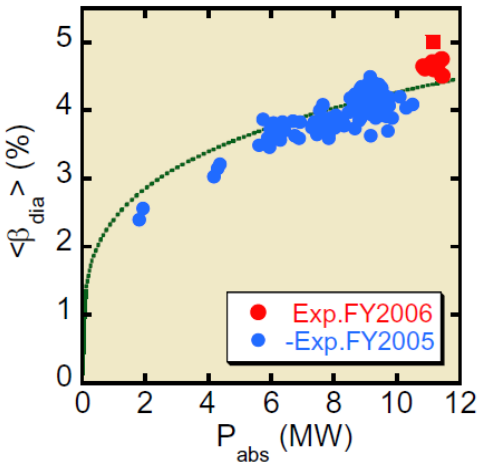

Fig.3 Volume-averaged beta value, <β>, as a function of the NBI-absorbed power.

With only the gas puffing, 4.8% of <β> was stationary sustained without any disruptive phenomena as shown in Fig. 2. The Shafranov shift normalized by the effective plasma minor radius is as large as around 40%, approaching the equilibrium beta limit of 50%. Although the MHD modes excited in the peripheral region with the magnetic hill are dominantly observed, they become stable spontaneously from the inner region to the outer region as the <β> increases. According to the linear MHD analysis, the Mercier criterion is not violated, and the observed peripheral MHD modes in the magnetic hill region is not crucial due to the strong magnetic shear there [18].

Even in the highest-β plasma, as described above, the MHD instabilities do not limit the achievable beta, but the heating power does. As shown in Fig. 3, the <β> is increased linearly to the 0.25 power of the NBI absorption power without saturation. The deduced absorbed power dependence of the <β> from the energy confinement scaling ISS95 is $P_{abs}^{0.4}$, and, thus, confinement degradation from the scaling law is suggested in the high <β> plasmas. The peripheral transport is enhanced with increasing the <β>. The dependence of the magnetic fluctuation resonated with the peripheral rational surfaces on the magnetic Reynolds number, S, suggests that the observed MHD modes are resistive interchange modes [19]. Thus, the resistive g-mode turbulence would cause the transport enhancement. Since the S is proportional to $B_t T_e^{3/2} n_e^{-1/2}$, the MHD mode amplitude is expected to be reduced for plasmas with higher temperature at higher magnetic field, relevant to the reactor-class plasma conditions. Another possible cause for the confinement degradation is the increase in the effective helical ripple due to the Shafranov shift [20]. The real-time control of the magnetic axis position during the discharge is planned, and that should resolve this issue. That should also be effective to

enhancement of the heating power by the perpendicular NBI, and then the further increase in the <β> is expected.

4. Extension of Operational Regime in High-Density Plasmas with Internal Diffusion Barrier

Formation of the super-dense core (SDC) plasma with the internal diffusion barrier (IDB) is a distinguished feature in LHD, which has been never observed in tokamaks. The IDB is originally formed in the LID-controlled plasmas which are fueled directly in the core region by the repetitive pellet injection. The LID functions as a strong pumping, which realizes a low recycling condition through the particle control at the plasma edge. Even in the helical divertor (HD) configuration, intensive wall conditioning should lead to a pumping by the wall. In the outward-shifted configuration, localization of the neutrals is small, and the recycling is suppressed due to weaker plasma-wall interaction. We have realized the IDB formation in the HD configuration in the outward-shifted configuration with such a kind of well-conditioned wall.

Figure 4 shows typical waveforms of an SDC plasma with the IDB realized in the HD configuration. The preset vacuum-magnetic axis position, R_{ax}^{vac}, is 3.8m. During the repetitive pellet injection into the plasma heated with high-power NBI, the electron density is greatly increased and the central density exceeds $5x10^{20}m^{-3}$. After the core

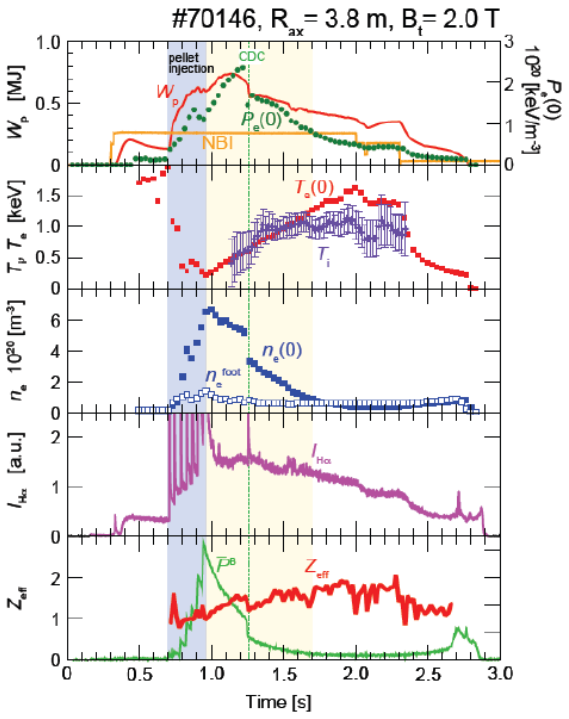

Fig.4 Typical waveforms of the SDC/IDB plasma formed in the HD configuration.

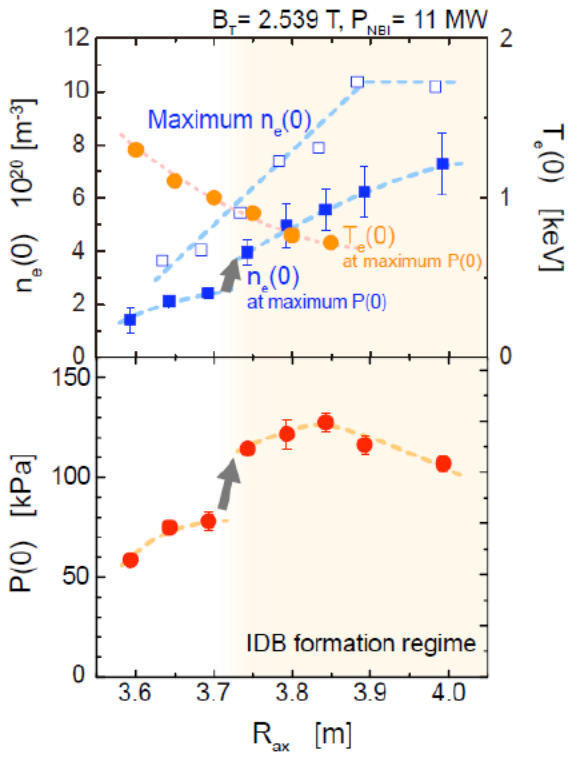

Fig.5 Maximum central density, $n_e(0)$, and pressure, P(0), as a function of the preset vacuum-magnetic axis position, R_{ax}^{vac}.

fueling with the pellet injection, the peripheral density is rapidly decreased in the density relaxation and temperature recovery phase, and, then, the SDC plasma with the IDB is formed. The central pressure continues to be still increased after the plasma stored energy turns to be decreased, and, occasionally, the core density collapse (CDC) occurs with an abrupt decrease in the central pressure as well as the central density. The impurity accumulation is not observed and the Z_{eff} is as low as around 1.5 during the discharge.

A series of the SDC/IDB experiments were performed in the HD configuration with a variation of the R_{ax}^{vac}, and the results are shown in Fig. 5. The formation of the IDB is definitely observed in the outward-shifted configuration at R_{ax}^{vac}>3.7m. The achieved central density, $n_e(0)$, is increased as the R_{ax}^{vac} is shifted more outward, and reaches $1x10^{21}m^{-3}$ at R_{ax}^{vac}=3.9m, while the peripheral density is maintained low, independent of the R_{ax}^{vac}. The central pressure, P(0), jumps up at the IDB formation, and the maximum P(0) is 130kPa, exceeding an atmospheric pressure, at R_{ax}^{vac}=3.85m.

The IDB formation is closely correlated with the edge-region temperature, which is strongly affected by the neutral density there. An increase in the neutral pressure in the SOL region causes an increase in the edge density with enhanced recycling, leading to a decrease in the edge temperature. Then, the heating power is lost by enhanced

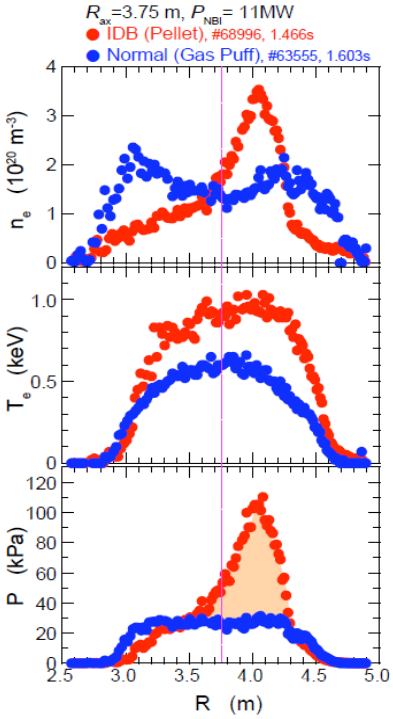

Fig.6 Comparison of the density, temperature, and pressure profiles of the SDC/IDB plasma with those of the gas-puffing plasma with no IDB. R_{ax}^{vac}=3.75m.

radiation in the low temperature region, resulting in the radiative collapse [21]. In the outward-shifted configuration, the recycling is suppressed compared with that in the inward-shifted configuration, and, thus, the low edge-density can be maintained by the wall-pumping effect without the LID. With a closed helical divertor system equipped with a strong pumping function, the stable IDB discharge would be realized even in the inward-shifted configurations.

Comparison of the pressure profile of the SDC/IDB plasma with that of the normal gas-puffing plasma at R_{ax}^{vac}=3.75m is shown in Fig. 6. The magnetic field strength on the axis and the NBI power are the same for both plasmas, and 2.539T and 11MW, respectively. Although the central density is about 2 times higher, the electron temperature is also higher in the SDC/IDB plasma. As a result, the central pressure is much higher with a steep pressure profile, indicating the confinement improvement in the SDC/IDB plasma. In the peripheral region, low density is maintained, leading to high T_e-gradient toward the core in the SDC/IDB plasma. On the other hand, since the peripheral density is high and the T_e-gradient region is narrow, the core T_e is low in the normal plasma. The central beta value, β(0), reaches 4.5% even at the high confinement magnetic field, and a large Shafranov shift of about 0.3m is observed due to the high central pressure with a peaked profile. The achievable β(0) is higher at lower confinement magnetic field, and 5.8% is observed at B_t=1.5T. The Shafranov shift is approaching to the equilibrium beta limit of 50% of the effective minor radius. The CDC event shown in Fig. 4 occurs when the Shafranov shift is so large that the shifted axis position would exceed R=4.0m. Vertically elongated modification by the ellipticity change of the magnetic surface is applied to suppress the Shafranov shift, and the CDC event is mitigated. The real-time control of the magnetic axis position by the dynamic control of the vertical field should be effective to improve the SDC/IDB plasma properties.

The achievable plasma stored energy of the SDC/IDB plasmas in outward-shifted configurations is linearly dependent on the plasma volume at the preset vacuum magnetic axis position, R_{ax}^{vac}, including the non-IDB plasmas in inward-shifted configurations. The plasma volume is smaller as the magnetic axis shifts more outward. Considering that the actual plasma volume is smaller due to the large Shafranov shift in the SDC/IDB plasmas, the plasma confinement is thought to be improved in the SDC/IDB plasmas.

Compared with the high-β plasma at the low magnetic field, the SDC/IDB plasma has a similar central beta, a steeper pressure gradient, and a larger Shafranov shift. The

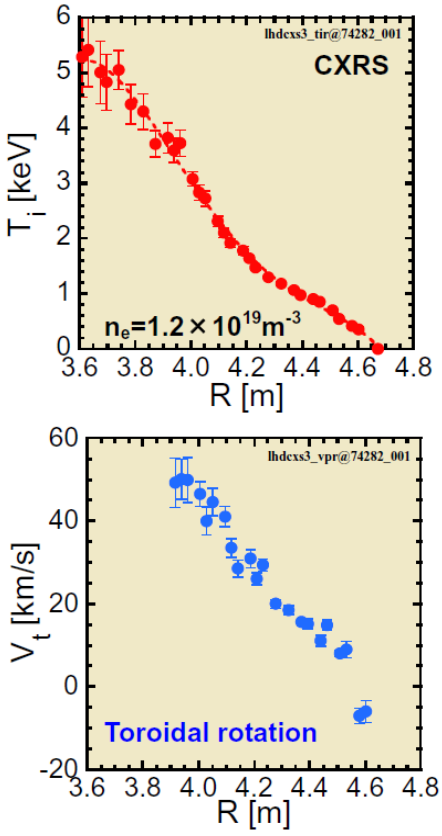

Fig.7 Profiles of the ion temperature and the toroidal rotation velocity in the high-T_i plasma.

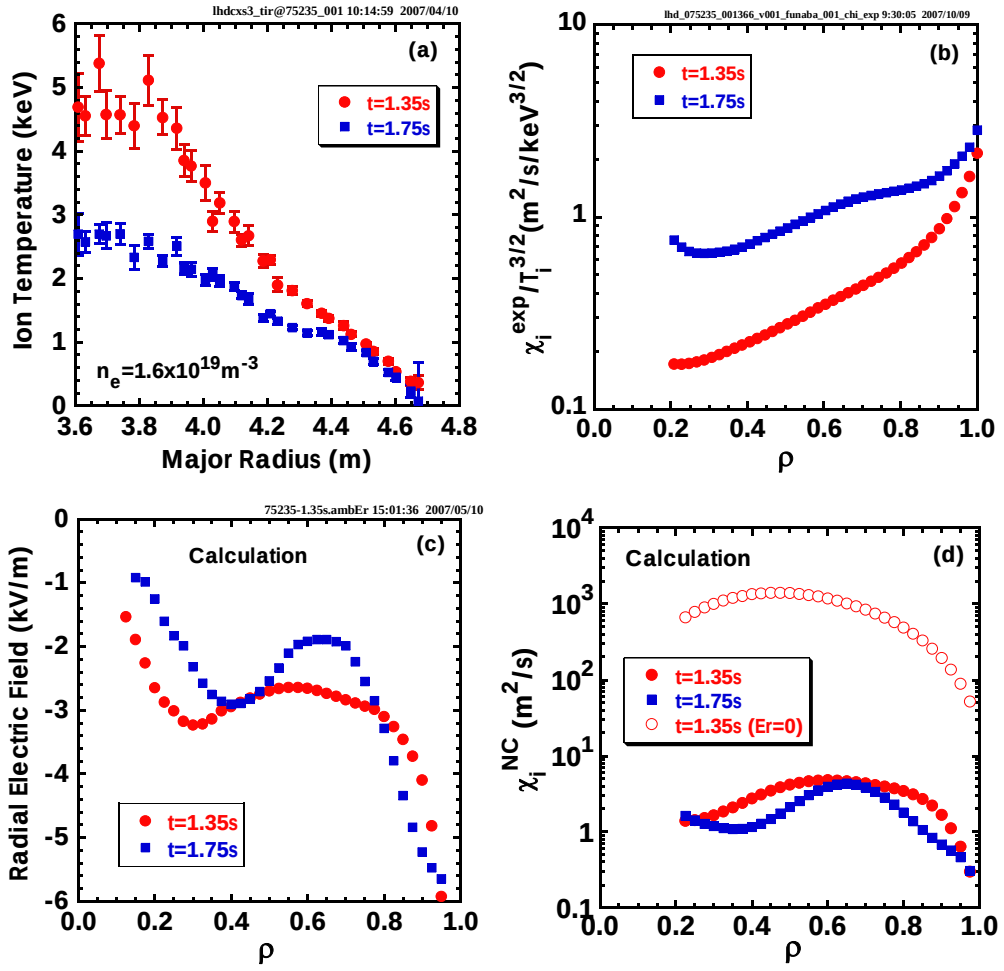

Fig.8 (a) T_i profiles, (b) ion thermal diffusivities divided by the gyro-Bohm factor, $\chi_i/T_i^{3/2}$, (c) radial electric field, E_r, obtained with the neoclassical ambipolar calculation, and (d) neoclassical ion thermal diffusivities, χ_i.

finite-β equilibrium in the SDC/IDB plasma at R_{ax}^{vac}=3.85m is investigated, using the HINT2 equilibrium code in which the nested magnetic surface is not assumed. The preliminary results show that due to the large Shafranov shift the magnetic surfaces are distorted in the peripheral region surrounding the IDB, and that inside the IDB the magnetic surfaces are clearly closed. Since the connection lengths of the magnetic field lines are much longer than the electron mean-free paths even in the region of the distorted magnetic surfaces, it is possible for the electron temperature profile to have a gradient. These analyses of the MHD equilibrium for the SDC/IDB plasmas should apply to the reactor-relevant high-β plasmas.

5. Increase in Ion Temperature and the Related Ion Transport

The high-energy NBI, which is the main heating device in LHD, dominantly heats electrons, and, thus, the high-Z discharge was utilized for the high-T_i experiments in LHD to increase effectively the ion heating power. As a result, the T_i was increased with an increase in the ion heating power, and reached 13.5keV at 0.3x10^{19}m^{-3} with Ar-gas puffing [22]. To apply this result to the hydrogen discharge, a low-energy NBI system with a radial injection, which dominantly heats ions, has been installed, and 40keV-6MW injection was achieved in the last experimental campaign [14,23]. This radially injected beam is also utilized for the T_i-profile measurement with the CXRS along a toroidal line of sight, which is better for the measurement in the central region than that along a poloidal line of sight [24].

With combination of the high-energy NBI and the low-energy NBI, 5.2keV of the ion temperature is obtained at 1.2x10^{19}m^{-3} as shown in Fig. 7. The density profile tends to be peaked by the low-energy NBI and to be flat or hollow by the high-energy NBI. The peaked density profile seems to be preferable for the T_i rise, suggesting a role of the fueling effect and/or the inward pinch effect with the low-energy NBI. Figure 7 also shows a profile of the

toroidal rotation velocity, V_t. The toroidal rotation is enhanced in the same direction as the dominant direction of the tangential NB injectors. As shown in Fig. 7(b), large V_t of 50km/s and the V_t shear are observed in the core region accompanied by the T_i rise. That suggests a correlation between the ion transport improvement and the toroidal rotation.

Figure 8 shows the results of the transport analysis. The ion thermal diffusivities normalized by $T_i^{3/2}$ of the gyro-Bohm factor are shown in Fig. 8(b) for the plasmas in Fig. 8(a). It is found that the $\chi_i/T_i^{3/2}$ is much reduced in the T_i rise to 5keV. As shown in Fig. 8(c), the neoclassical ambipolar calculation shows negative E_r in the core region in association with the T_i rise [25], meaning that the T_i is increased in the neoclassical ion root. The calculated neoclassical χ_i is shown in Fig. 8(d). Without consideration of the E_r effect, the ripple transport is greatly enhanced by the T_i rise, and it is found that by the negative E_r the ripple transport is greatly reduced. As a result, the neoclassical χ_i is not so changed by the T_i rise. Considering that the experimental $\chi_i/T_i^{3/2}$ is much reduced, the experimental improvement of the ion confinement is due to the reduction of the anomalous transport in the ion root. The negative E_r is induced by the increased ion temperature, and a role of the negative E_r in the reduction of the anomalous transport should be investigated.

The CXRS intensity profile of the CVI emission shows that the carbon impurity profile becomes strongly hollowed as the T_i is increased. This "impurity hole" is clearly observed in the plasmas with the carbon pellet injection. After the carbon pellet injection, the T_i is increased in the density-decay phase, and the carbon density ratio is rapidly decreased to 0.2% at the plasma center while it is 10% at the edge. As a result, the T_i measurement in the core region becomes impossible. The outward flux of carbon is observed even at a negative carbon-density gradient. In the neoclassical theory, the outward flow of impurities is predicted in the electron root with positive E_r, and the impurity pump-out effect is observed in the ECRH plasmas. However, the "impurity hole" is observed in the ion-root plasma with negative E_r. The physics of the "impurity hole" in the high-T_i plasmas should be investigated as an inherent subject in the helical systems.

On the other hand, the T_i rise is observed also in the electron root. When the ECRH is superposed on the NBI-heated plasma, the T_i is increased accompanied by the formation of the electron-ITB with positive E_r [22]. The transport analysis indicates that both electron and ion transport is improved in the core region with the reduction of the anomalous transport. The toroidal rotation is driven in the co-direction by adding the ECRH, and the spontaneous toroidal rotation is suggested to be related to

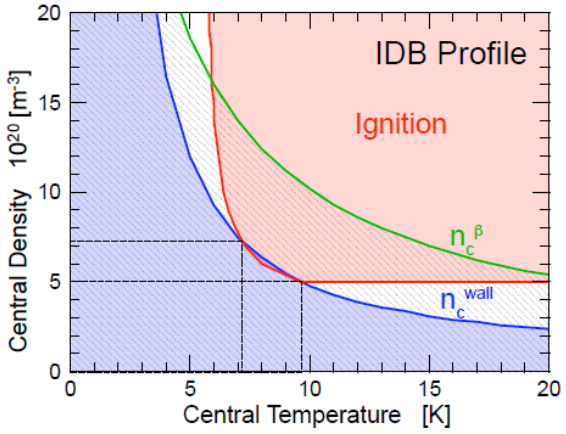

Fig.9 Operational regime for the high-density ignition based on the IDB profile in the helical reactor.

the transport improvement in the electron-root plasma [26]. Although the electron transport improvement is a common feature in the CERC (core electron-root confinement) plasmas [27], the ion transport improvement in the CERC suggests a possible approach to achieve the reactor-relevant high-temperature plasmas.

6. High-Density Ignition Scenario for a Helical Fusion Reactor

For the steady-state helical fusion reactor, a novel ignition approach based on the high-density SDC/IDB plasma is proposed. Figure 9 shows the operational regime for the self-ignition based on the high-density IDB profile in the helical reactor. In tokamaks, since high-density operation is limited by the current drive condition and the MHD stability, a high-temperature path at relatively low density is the possible ignition scenario. On the other hand, LHD is capable to achieve high-density plasmas above $5x10^{20}m^{-3}$ without any limitation, and, based on this high-density plasma, the required temperature for the ignition, then, should be reduced below 10keV. This scenario is advantageous to the helical devices which require no current drive. The operation at a relatively high collisionality mitigates the helical ripple transport, and the engineering demand derived from the high-temperature operation is reduced. In the peripheral region of the SDC/IDB plasma, a temperature gradient is established due to the low density there, and the core temperature high enough to realize the ignition is achieved by this temperature gradient. Maintaining the low density in the peripheral region is also desirable for avoiding the radiative collapse as well as suppression of the enhanced synclotron radiation. At present, an LHD-type fusion reactor is being designed based on this high-density ignition scenario [9].

7. Concluding Remarks

Recent extension of the operational regime in the LHD experiments is reviewed together with the progress of the physics understanding. By the sophisticated optimization of the magnetic field configuration with regard to the magnetic axis position and the plasma aspect ratio, the volume-averaged beta was increased to 5.0% with an increase in the NBI heating power. Even in this fusion-relevant high-β plasma, no crucial MHD instability is observed in the core region while the resistive interchange modes degrade the plasma confinement in the peripheral region. However, these MHD modes should be stabilized in reactor-relevant plasmas with higher temperature at higher magnetic field.

The SDC/IDB plasmas, which were originally observed in the LID configuration, were realized in the helical divertor configuration. The central density is increased as the preset vacuum-magnetic axis position is shifted outward, and reaches $1x10^{21}m^{-3}$ at R_{ax}^{vac}=3.9m. The central pressure exceeds an atmospheric pressure and reaches 130kPa. The core plasma confinement is improved while the particle transport in the peripheral plasma surrounding the IDB is degraded. This, in turn, realizes the low density with an electron temperature gradient in the peripheral region. The Shafranov shift due to the high central beta and the steep pressure gradient is approaching the equilibrium limit, leading to the core density collapse occasionally. The dynamic control of the magnetic axis position by the vertical field is required as well as in the high-β plasmas.

For an increase in the ion heating power, a low-energy NB injector was newly installed, and 40keV-6MW injection was achieved. The ion temperature is raised to 5.2keV at $1.2x10^{19}m^{-3}$ with the combined heating of the low-energy NBI and the high-energy NBI. The ion transport is improved with the reduction of the anomalous transport in the neoclassical ion root. An increase in the toroidal rotation is observed to be related to the ion-temperature rise. The impurity hall is recognized, in which the carbon impurity is drastically decreased in the core region with an increase in the T_i. The impurity pump-out effect in the ion root is attractive for the helical reactor because no impurity accumulation is expected in the high-T_i core plasma.

The SDC/IDB high-density plasma allows us to propose a high-density ignition scenario. In this ignition approach the temperature requirement is reduced below 10keV at a high-density above $5x10^{20}m^{-3}$, and the helical ripple transport is mitigated together with the reduction of the engineering demand caused by the high-temperature operation. Including this scenario, most of the LHD results presented here are relevant to the steady-state helical fusion reactor, and the upgrade of the LHD is now planned including the deuterium experiments for investigations of the high-performance plasmas, which should lead to a definite design of the LHD-type fusion reactor.

Acknowledgements

The authors greatly acknowledge all contributions from overseas and domestic collaborators for the progress of the LHD achievements. They are also grateful to the technical staff in the LHD for the excellent operation of the LHD and the heating systems.

References

[1] A. Iiyoshi, *et al.*, Fusion Technol. **17**, 169 (1990).
[2] A. Iiyoshi, *et al.*, Nucl. Fuion **39**, 1245 (1999).
[3] O. Motojima, *et al.*, Nucl. Fuion **40**, 599 (2000).
[4] A. Komori, *et al.*, Fusion Sci. Technol. **50**, 136 (2006).
[5] O. Motojima, *et al.*, Nucl. Fusion **47**, S668 (2007).
[6] N. Ohyabu, *et al.*, Phys. Rev. Lett. **97**, 055002 (2006).
[7] A. Komori, *et al.*, Nucl. Fusion **45**, 837 (2005).
[8] R. Sakamoto, *et al.*, Nucl. Fusion **46**, 884 (2006).
[9] A. Sagara, *et al.*, this conference.
[10] T. Mutoh, *et al.*, Nucl. Fusion **47**, 1250 (2007).
[11] H. Yamada, *et al.*, Plasma Phys. Control. Fusion **43**, A55 (2001).
[12] O. Kaneko, *et al.*, *Proc. 16th Int. Conf. on Fusion Energy 1996 (Montreal, 1996)* Vol. 3 (Vienna, IAEA) p. 539.
[13] Y. Takeiri, *et al.*, Nucl. Fusion **46**, S199 (2006).
[14] M. Osakabe, *et al.*, this conference.
[15] S. Kubo, *et al.*, Plasma Phys. Control. Fusion **47**, A81 (2005).
[16] T. Mutoh, *et al.*, Nucl. Fusion **43**, 738 (2003).
[17] K.Y. Watanabe, *et al.*, Nucl. Fusion **45**, 1247 (2005).
[18] S. Sakakibara, *et al.*, *Proc. 21st IAEA Conf. on Fusion Energy (Chengdu, 2006)*, IAEA-CN-149, EX/7-5 (2006).
[19] S. Sakakibara, *et al.*, Fusion Sci. Technol. **50**, 177 (2006).
[20] H. Yamada, *et al.*, Nucl. Fusion **45**, 1684 (2005).
[21] J. Miyazawa, *et al.*, Plasma Phys. Control. Fusion **48**, 325 (2006).
[22] Y. Takeiri, *et al.*, Nucl. Fusion **47**, 1078 (2007).
[23] K. Nagaoka, *et al.*, this conference.
[24] M. Yoshinuma, *et al.*, this conference.
[25] S. Matsuoka, *et al.*, this conference.
[26] Y. Takeiri, *et al.*, this conference.
[27] M. Yokoyama, *et al.*, Fusion Sci. Technol. **50**, 327 (2006).